Kinetic Theory Analysis for the Flowfield of a Two-Dimensional Nozzle Exhausting to Vacuum

A. A. PERACCHIO*
United Aircraft Research Laboratories, East Hartford, Conn.

An analytical study is presented based on the BGK equation. The nonlinear BGK equation is solved iteratively by integration through use of the method of characteristics. A computer program based on the resulting equations is described and plots of density, temperature, and velocity for the exhaust region are shown for two nozzle Reynolds numbers (or chamber pressures). As expected, the results deviate from continuum predictions. The flowfield exists everywhere, not only within the limiting streamline predicted by continuum theory. More importantly, an unexpected rise in static temperature is noted in the expansion flowfield near the corner of the nozzle where the largest deviations from the assumptions of continuum fluid mechanics occur.

Nomenclature

A = constant in BGK equation
$\bar{A}$ = AL/V_0
$ANG(J)$ = ϕ
B_1 = $[\gamma/(\gamma-1)(1/\bar{T})]^{1/2}(V_x\cos\alpha + V_y\sin\alpha)$
$B_{\Gamma 1}$ = $[\gamma/(\gamma-1)(1/\bar{T}_\Gamma)]^{1/2}V_{y\Gamma}\cos\alpha$
C_1 = $[\gamma/(\gamma-1)(1/\bar{T})]^{1/2}\int_0^\eta \bar{A}d\eta$
$C_{\Gamma 1}$ = $[\gamma/(\gamma-1)(1/\bar{T}_\Gamma)]^{1/2}\int_0^{\eta_0}\bar{A}d\eta$
d^3u = elemental volume in velocity space
$d\tau$ = elemental volume in physical space
F = maxwellian distribution function
$\bar{F}$ = $\int F dw$
f = distribution function
f_Γ = value of f on nozzle boundary
$\bar{f}$ = $\int f dw$
$\bar{f}_\Gamma$ = value of $\bar{f}$ on nozzle boundary
G = $\int w^2 F dw$
g = $\int w^2 f dw$
$g_n(C,B)$ = $\int_0^\infty Zn\exp\left\{-(B-Z)^2 - \frac{C}{Z}\right\}dZ$
g_Γ = value of g on nozzle boundary
I_ρ, I_T = integral operators for $\bar{\rho}$, $\bar{T}$, $\bar{V}_x$, and $\bar{V}_y$, respectively
I_{vx}, I_{vy}
L = nozzle exit half width
m = molecular mass
P_0 = chamber pressure
R = gas constant
R_M = maximum radius of flowfield
$R(I)$ = radial location of mesh point
R_{e0} = nozzle Reynolds number $= \rho_0 V_0 L/\mu_0$
T = static temperature
T_0 = chamber or nozzle exit total temperature
T_Γ = static temperature at nozzle exit
$\bar{T}$ = T/T_0
$\bar{T}_\Gamma$ = T_Γ/T_0
u = u_1/V_0
u_i = molecular velocity vector
u_1, u_2, u_3 = x_1, x_2, x_3 components of molecular velocity
V = magnitude of molecular velocity
$V_i, \mathbf{V}_0$ = macroscopic velocity vector
V_0 = maximum isentropic velocity
V_x, V_y = V_1/V_0, V_2/V_0, respectively
$V_{y\Gamma}$ = nozzle exit velocity
$\bar{V}_{y\Gamma}$ = $V_{y\Gamma}/V_0$
v = u_2/V_0
w = u_3/V_0
x = x_1/L
x_1, x_2, x_3 = cartesian coordinates of physical space
x_Γ = x coordinate of point on boundary
y, z = x_2/L, x_3/L respectively
y_Γ = y coordinate of point on boundary
α = angle between V_i and x axis; direction of characteristic line
γ = ratio of specific heats
$\mathfrak{F}$ = partial distribution function
η = distance measured from (x,y) along a characteristic
η_0 = distance from (x,y) to (x_Γ, y_Γ)
η' = variable of integration, physically equivalent to η
μ = coefficient of viscosity or angle between $\mathbf{V}_0$ and x axis
ρ = density
ρ_0 = nozzle chamber density
$\bar{\rho}_\Gamma$ = nozzle exit density
$\bar{\rho}, \bar{\rho}_\Gamma$ = $\bar{\rho}/\rho_0$, $\bar{\rho}_\Gamma/\rho_0$, respectively
ϕ = angle between y axis and radius vector
ω = exponent in relationship between viscosity and temperature

Presented as Paper 69-658 at the AIAA Fluid and Plasma Dynamics Conference, San Francisco, California, June 16–18; submitted June 10, 1969; revision received December 2, 1969. This paper summarizes a doctoral thesis submitted to Rensselaer Polytechnic Institute, Troy, N. Y., May 1968, and was supported by the Hamilton Standard Division of United Aircraft Corporation.

* Senior Research Engineer. Member AIAA.

Introduction

THE venture of man into space has led to the need for specifying the flowfield of rockets exhausting to vacuum. The use of continuum fluid mechanics for prediction of the complete exhaust plume flowfield of such rockets is invalid. For example, continuum theory predicts a limiting stream surface beyond which no flow exists, whereas considerations at the molecular level show this to be unrealistic. Furthermore, deviations arise due to the large gradients generated by the rapid expansion at the nozzle corners. In addition, the flowfield spans the continuum, transition, and free molecular regimes. Therefore a solution to the problem valid for the entire flowfield requires recourse to the kinetic theory of gases, which is not limited by continuum considerations.

A certain class of expansion flows has been considered in the literature. For example, solutions of the hypersonic moment equations, for the "outer" regions of the plume have been patched to isentropic "inner" solutions.[1] The resulting total solution is not valid for streamlines near the edge of the nozzle, since here dissipation effects occur in the "inner" flowfield, violating the isentropic flow assumption.

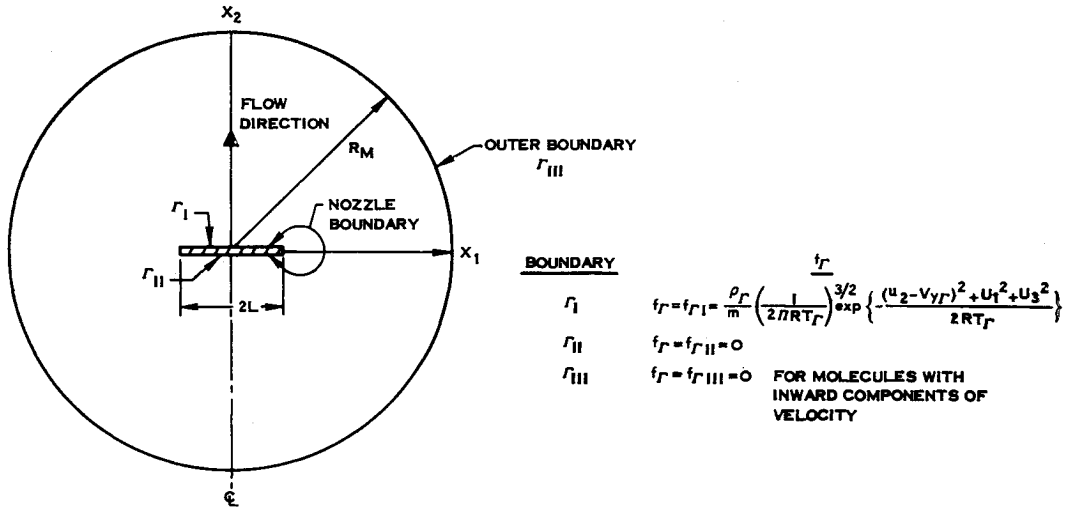

Fig. 1 Flowfield boundary conditions.

A similar patching procedure has been applied to the solution of the supersonic source.[2,3] This problem has been also solved by direct application of the BGK (Bhatnagar-Gross-Krook) equation,[4] but all solutions are one dimensional, allowing for radial variations only. The present work predicts the two-dimensional flowfield of a nozzle exhausting to vacuum by application of the BGK equation. The two-dimensional nature of the flow is therefore accounted for and the solution is valid everywhere, since the assumptions of isentropic or hypersonic flow are not required.

Problem Definition

The steady flow from a nozzle into a vacuum will be solved by application of the BGK equation.[5,6] Due to the complexities of the numerical solution, especially in terms of computer time, the case of a two-dimensional nozzle will be considered. This problem still retains all the features of interest and can also serve as the basis for a three-dimensional solution should it be needed. Particular emphasis will be placed on the definition of the flow in the vicinity of the free streamline and in the corner of the nozzle where large gradients in density, temperature, and velocity are likely to cause significant deviations from the isentropic solution.

The Distribution Function

Kinetic theory studies the molecular behavior of a gas by use of the distribution function, f, which is defined as the number of molecules per unit volume at the point (x_i,u_i) of phase space. The density of the fluid at x_i is

$$\rho(x_i) = m\int\!\!\!\int\!\!\!\int f d^3u \tag{1}$$

where the shorthand notation $\int\!\!\!\int\!\!\!\int f d^3u$ is used for the triple integral

$$\int_{-\infty}^{\infty}\int_{-\infty}^{\infty}\int_{-\infty}^{\infty} f du_1 du_2 du_3$$

The macroscopic velocity and temperature become, in terms of f,

$$\rho V_i = m\int\!\!\!\int\!\!\!\int u_i f d^3u \tag{2}$$

$$3\rho RT = m\int\!\!\!\int\!\!\!\int (u_i - V_i)(u_i - V_i) f d^3u \tag{3}$$

The BGK equation, which defines the behavior of f, is given as[6]

$$u_i \partial f/\partial x_i = A[F - f] \tag{4}$$

The constant A is proportional to density and is a measure of the collision frequency. The details of the collision process are incorporated into the BGK expression through this constant. F represents the Maxwellian or equilibrium distribution function based on the local values of density, temperature and velocity and is given as

$$F(\rho,V_i,T,u_i) = \rho/m(1/2\pi RT)^{3/2} \exp\{-(u_i - V_i)^2/2RT\} \tag{5}$$

Solution of the BGK Equation

Boundary Conditions

Before the BGK equation can be solved it is necessary to specify a set of boundary conditions for the distribution function, f. In order to simplify the geometry of the problem, the two-dimensional nozzle is represented as a one-sided line source of width $2L$ in the x_1, x_2 plane (see Fig. 1). The flow is assumed to leave the nozzle in the positive x_2 direction, thereby making the upper half plane the region of primary interest. Note that the nozzle external shape in the lower half plane is not properly accounted for with the line representation. This has a negligible effect on the region of the flowfield of major interest, which lies in the upper half plane, since in the lower half plane the collision frequency is so low that the number of molecules reaching the upper half plane is negligible.

The flow leaving the nozzle exit plane is assumed to have expanded isentropically to the exit Mach number dictated by the nozzle area ratio. The boundary layer at the nozzle exit is neglected. Within this framework, the properties of the fluid at the nozzle exit are uniform and given by the isentropic flow relations in terms of the nozzle area ratio. Consistent with this description, the distribution function at the nozzle exit is taken to be the Maxwellian distribution based on the exit temperature, density, and velocity. Thus f_Γ, the value of f on the nozzle boundary, is given as

$$f_\Gamma = \rho_\Gamma/m(1/2\pi RT_\Gamma)^{3/2} \exp\{-[(u_2 - V_{y\Gamma})^2 + u_1^2 + u_3^2]/2RT_\Gamma\} \tag{6}$$

The value of f on the lower side of the line, for simplicity is chosen to be zero, implying that any molecules that reach it are absorbed and never return to the flow. Again, the effect of this assumption on the flowfield in the upper half plane is negligible.

The actual flowfield extends to infinity in all directions. The solution considered here will be limited to the finite region of the (x_1,x_2) plane defined by a circle of radius, R_M, as shown in Fig. 1, and therefore requires the specification of f along R_M.

In general, the value of f along R_M depends on the flow properties along R_M. As R_M gets large, the velocity vector tends to become radially oriented, with its magnitude equal to the maximum velocity consistent with the chamber total temperature, while the temperature either decreases or reaches some limiting value. Thus the Mach number along R_M, at least in the upper half plane, will be quite large. This means that most of the molecules are directed in the radially outward direction, and only a negligible number of molecules are inwardly directed. This is tantamouut to imposing the hypersonic limit on the moment equations as discussed by Hamel and Willis,[3] and Edwards and Rogers,[1] where the distribution function, at high Mach numbers, is seen to approximate a delta function about the macroscopic velocity vector. Applying this observation to the problem at hand it is clear that some value of radius R_M exists beyond which the Mach number is high and the velocity vector is oriented in an essentially radial direction, so that a negligible number of molecules have an inward component of velocity. As a result of the above argument and the low densities in the lower half plane, the value of f on R_M is set equal to zero.

In summary, then, the nozzle is represented as a one-sided line source in the (x_1,x_2) plane whose length is $2L$ as shown in Fig. 1. In addition, solutions to the flowfield are sought only in a region bounded by a circle of radius R_M which is chosen large enough to guarantee the required directionality to the distribution function. The boundary condition of f along these boundaries is specified so that on the upper half of the line the distribution is Maxwellian and is based on nozzle exit properties consistent with isentropic flow through the nozzle. The value of f on the lower half of the slit is zero and the value of f on R_M is zero for molecular velocities with a radially inward component. The flowfield geometry and boundary conditions are summarized in Fig. 1.

Nondimensional BGK Equation

In what follows, a nondimensional version of the BGK equation will be developed and used. The space variables (x_1,x_2) will be nondimensionalized with respect to L. The density and temperature will be nondimensionalized with respect to chamber density and temperature, ρ_0 and T_0. The velocity vector will be nondimensionalized with respect to maximum velocity, V_0, which is defined as the velocity attained by isentropic expansion from chamber conditions to zero pressure. The distribution function is not nondimensionalized since it will be eliminated from the analysis at a later point. The BGK equation in nondimensional form becomes

$$u\partial f/\partial x + v\partial f/\partial y = \bar{A}[F - f] \tag{7}$$

where $\bar{A} = AL/V_0$ and $f = f(x,y,u,v,w)$. The Maxwellian distribution function F becomes, in terms of nondimensional density, temperature and velocity,

$$F = \frac{\rho_0}{m}\frac{1}{(2\pi RT_0)^{3/2}}\times \frac{\bar{\rho}}{\bar{T}^{3/2}}\exp\left\{-\frac{\gamma}{\gamma-1}\frac{1}{\bar{T}}([u-V_x]^2+[v-V_y]^2+w^2)\right\} \tag{8}$$

The moments of f must also be written in terms of the nondimensional coordinates. Thus,

$$\bar{\rho} = \frac{mV_0^3}{\rho_0}\int f du dv dw \tag{9}$$

similarly,

$$\bar{\rho}\begin{Bmatrix}V_x\\V_y\end{Bmatrix} = \frac{mV_0^3}{\rho_0}\int\begin{Bmatrix}u\\v\end{Bmatrix} f du dv dw \tag{10}$$

$$\tag{11}$$

$$\bar{\rho}\bar{T} = \tfrac{2}{3}m\left(\frac{\gamma}{\gamma-1}\right)\frac{V_0^3}{\rho_0}\int[(V_x-u)^2+(V_y-v)^2+w^2]f du dv dw \tag{12}$$

The parameter $\bar{A}$ can be written in terms of a Reynolds number for the nozzle and becomes

$$\bar{A} = [(\gamma-1)/2\gamma](Reo)\bar{\rho}\bar{T}^{1-\omega}$$

A complete description of the above derivation is given by Peracchio.[7]

Reduction of BGK Equation to Four Independent Variables

It is now possible to eliminate w from the above equations, thereby reducing the number of independent variables to four. This is accomplished at the expense of an additional unknown dependent variable whose behavior is defined by an equation very similar to the BGK equation and, as will be seen, requires very little extra effort for its evaluation. The method used follows that of Chu[8] for one-dimensional flows and Anderson[9] for two-dimensional flows. The variable w, representing the z component of the molecular velocity does not appear explicitly on the left-hand side of the BGK equation. Further, since V_z is zero and variations in the z direction are zero, the distribution function must be symmetrical with respect to w. Thus

$$\int_{-\infty}^{\infty} wf(w)dw = 0 \tag{13}$$

The independent variable w is now eliminated from the BGK equation and f. First, integrate the BGK equation over w, which by defining a new pseudo-distribution function $\bar{f}$ as follows,

$$\bar{f}(u,v,x,y) = \int_{-\infty}^{\infty} f(u,v,w,x,y)dw \tag{14}$$

becomes

$$u\partial\bar{f}/\partial x + v\partial\bar{f}/\partial y = \bar{A}[\bar{F} - \bar{f}] \tag{15}$$

where $\bar{F}$ is defined as

$$\bar{F}(u,v,x,y) = \int_{-\infty}^{\infty} F(u,v,w,x,y)dw$$

Thus $\bar{f}$, $\bar{F}$ and Eq. (15) depended on the four variables $(u,v,x,y,)$, w having been eliminated by Eq. (14). The first two moments can be written in terms of $\bar{f}$ by integrating over w, i.e.,

$$\bar{\rho} = \frac{mV_0^3}{\rho_0}\int\bar{f}du dv \tag{16}$$

$$\bar{\rho}\begin{Bmatrix}v_x\\v_y\end{Bmatrix} = \frac{mV_0^3}{\rho_0}\int\begin{Bmatrix}u\\v\end{Bmatrix}\bar{f}du dv \tag{17}$$

$$\tag{18}$$

The equation for temperature, because of the w^2 term, cannot be completely integrated, i.e.,

$$\bar{\rho}\bar{T} = \tfrac{2}{3}(\gamma/\gamma-1)mV_0^3/\rho_0\{\int[(V_x-u^2)+(V_y-v)^2]\bar{f}du dv + \int w^2 f du dv dw\} \tag{19}$$†

It is the second integral in Eq. (19) that now presents a problem. This problem can be overcome by introducing a new variable g defined as follows:

$$g(u,v,x,y) = \int_{-\infty}^{\infty} w^2 f dw \tag{20}$$

† The first and second integrals in Eq. (19) are proportional to the parallel and perpendicular components of temperature used in the works of Hamel and Willis[3] and Edwards and Cheng.[2] In the present formulation, this distinction is not made, and only the temperature as defined by Eq. (19) is considered.

An equation governing the behavior of g can be derived by multiplying the BGK equation by w^2 and integrating over w. Using the definition of g, this equation becomes

$$u\partial g/\partial x + v\partial g/\partial y = \bar{A}[G - g] \tag{21}$$

where

$$G(u,v,x,y) = \int_{-\infty}^{\infty} w^2 F(u,v,w,x,y)dw$$

and is known, since the dependence of F on w is known. Equation (21) represents the desired equation for the behavior of g, and is of the same form as the BGK equation for $\bar{f}$. The equation for temperature now becomes

$$\bar{\rho}\bar{T} = \tfrac{2}{3}(\gamma/\gamma - 1)mv_0^3/\rho_0\{\int[(V_x - u)^2 + (V_y - v)^2]\bar{f}dudv + \int gdudv\} \tag{22}$$

The elimination of w as an independent variable has been accomplished at the expense of adding a new dependent variable, g, along with its governing equation, which, however, is of the same form as the BGK equation.

The forms of $\bar{F}$ and G can be obtained by direct integration and become

$$\bar{F} = \frac{1}{m}\frac{\rho_0}{(2\pi RT_0)^{3/2}}\frac{\bar{\rho}}{\bar{T}}\left(\frac{\gamma - 1}{\gamma}\pi\right)^{1/2} \times \exp\left\{-\frac{\gamma}{\gamma - 1}\frac{1}{\bar{T}}[(u - V_x)^2 + (v - V_y)^2]\right\} \tag{23}$$

$$G = \frac{1}{2m}\pi^{1/2}\left(\frac{\gamma - 1}{\gamma}\right)^{3/2}\frac{\rho_0}{(2\pi RT_0)^{3/2}} \times \bar{\rho}\exp\left\{-\frac{\gamma}{\gamma - 1}\frac{1}{\bar{T}}[(u - V_x)^2 + (v - V_y)^2]\right\} \tag{24}$$

The boundary value of $\bar{f}$, i.e., $\bar{f}_\Gamma$ is obtained in similar fashion.

Solution by the Method of Characteristics

Solution of the above set of equations by the method of characteristics is considered next. The solution will be discussed in terms of the BGK equation for $\bar{f}$, i.e., Eq. (15). The solution for g is exactly the same, since both equations are of the same form and have the same characteristics. Equation (15) is, in reality, a nonlinear integro-differential equation, since $\bar{F}$ depends on $\bar{\rho}$, $\bar{T}$, etc., which in turn depend on $\bar{f}$ through the moment equations.

The details of the integration procedure are given by Peracchio.[7] The results are shown below. The expression for $\bar{f}$ becomes, in terms of (V, α) the polar representation of molecular velocity,

$$\bar{f}(x,y,V,\alpha) = \left[\bar{f}_\Gamma + \frac{1}{V}\int_0^{\eta_0}\bar{A}(\eta,\alpha)\bar{F}(\eta,\alpha,V) \times \exp\left\{\frac{1}{V}\int_\eta^{\eta_0}\bar{A}d\eta'\right\}d\eta\right]\exp\left\{-\frac{1}{V}\int_0^{\eta_0}\bar{A}(\eta',\alpha)d\eta'\right\} \tag{25a}$$

where $\bar{A}$, $\bar{F}$ depend not only on η, distance along the characteristic, but also on α, the direction of the characteristic line through (x,y).

The equation for g [Eq. (21)], being of the same form as the equation for $\bar{f}$, has the same characteristic equation. The expression for g is derived in a fashion analogous to the expression for $\bar{f}$, and is

$$g(x,y,V,\alpha) = \left[g_\Gamma + \frac{1}{V}\int_0^{\eta_0}\bar{A}(\eta,\alpha)G(\eta,\alpha,V) \times \exp\left\{\frac{1}{V}\int_\eta^{\eta_0}\bar{A}(\eta',\alpha)d\eta'\right\}d\eta\right] \times \exp\left\{-\frac{1}{V}\int_0^{\eta_0}\bar{A}(\eta,'\alpha)d\eta'\right\} \tag{25b}$$

where g_Γ is the value of g at the intersection of the characteristic line and the boundary curve along which g is known.

In order to facilitate the simultaneous solution of Eqs. (25) and the moment equations for the flowfield properties, it is expedient to eliminate $\bar{f}$ and g from the moment equations, as outlined in the following section.

Substitution of $\bar{f}$ in the Equations for Density, etc.

Equations (25), as they stand, contain a mixed set of variables for velocity space. $\bar{F}$, as defined by Eq. (23), contains the cartesian components (u,v) whereas the rest of Eqs. (25) are in terms of (V,α). It is expedient, for the integrations over velocity space necessary for the evaluation of density, temperature, and velocity to use the (V,α) description of velocity space, since it then becomes possible to perform the integration over V a priori. If (u,v) is used, then the upper limit of integration $\eta_0(x,y,\alpha)$ in Eqs. (25) depends on both u and v since Tan $\alpha = v/u$ and integrations over velocity space must be performed after the integration over η. On the other hand, use of (V,α) eliminates V from the η limit of integration, and, in addition, the functional dependence of the integrand on V is known explicitly, thereby permitting the V integration to be performed. The form of the integrand and the method by which the integration over V is accomplished is given in detail by Peracchio.[7] Substituting $\bar{f}$ and g into the equations for density, temperature, and velocity, and utilizing the appropriate boundary conditions, Eqs. (26–29) are obtained

$$\pi\bar{\rho} \equiv \int_0^{2\pi}\bar{\rho}_\Gamma\exp\left\{-\frac{\gamma}{\gamma - 1}\frac{\bar{V}_{y\Gamma}^2\cos^2\alpha}{\bar{T}_\Gamma}\right\}g_1(C_{\Gamma 1},B_{\Gamma 1})d\alpha + \left(\frac{\gamma}{\gamma - 1}\right)^{1/2}\int_0^{2\pi}\int_0^{\eta_0}\frac{\bar{\rho}\bar{A}}{(\bar{T})^{1/2}} \times \exp\left\{-\frac{\gamma}{\gamma - 1}\frac{1}{\bar{T}}(V_x\sin\alpha - V_y\cos\alpha)^2\right\}g_0(C_1,B_1)d\eta d\alpha \tag{26}$$

$$\pi\bar{\rho}\begin{Bmatrix}V_x\\V_y\end{Bmatrix} = \int_0^{2\pi}\bar{\rho}_\Gamma\left(\frac{\gamma - 1}{\gamma}\bar{T}_\Gamma\right)^{1/2}\begin{Bmatrix}\cos\alpha\\\sin\alpha\end{Bmatrix}g_2(C_{\Gamma 1},B_{\Gamma 1}) \times \exp\left\{-\frac{\gamma}{\gamma - 1}\frac{\bar{V}_{y\Gamma}^2\cos^2\alpha}{\bar{T}_\Gamma}\right\}d\alpha + \int_0^{2\pi}\int_0^{\eta_0}\bar{A}\bar{\rho}\begin{Bmatrix}\cos\alpha\\\sin\alpha\end{Bmatrix} \times g_1(C_1,B_1)\exp\left\{-\frac{\gamma}{\gamma - 1}\frac{1}{\bar{T}}(V_x\sin\alpha - V_y\cos\alpha)^2\right\}d\eta d\alpha \tag{27}$$

(28)

$$\frac{3}{2}\pi\bar{\rho}\bar{T} = \int_0^{2\pi}\left[\bar{\rho}_\Gamma\exp\left\{-\frac{\gamma}{\gamma - 1}\frac{1}{\bar{T}_\Gamma}\bar{V}_{y\Gamma}^2\cos^2\alpha\right\} \times \left\{\bar{T}_\Gamma(g_3(C_{\Gamma 1},B_{\Gamma 1}) + \frac{1}{2}g_1(C_{\Gamma 1},B_{\Gamma 1})) + \frac{\gamma}{\gamma - 1} \times (V_x^2 + V_y^2)g_1(C_{\Gamma 1},B_{\Gamma 1}) - 2(V_x\cos\alpha + V_y\sin\alpha) \times \left(\frac{\gamma}{\gamma - 1}\bar{T}_\Gamma\right)^{1/2}g_2(C_{\Gamma 1},B_{\Gamma 1})\right\}\right]d\alpha + \int_0^{2\pi}\int_0^{\eta_0} \times \left[\bar{A}\bar{\rho}\exp\left\{-\frac{\gamma}{\gamma - 1}\frac{1}{\bar{T}}(V_x\sin\alpha - V_y\cos\alpha)^2\right\} \times \left\{\left(\frac{\gamma}{\gamma - 1}\bar{T}\right)^{1/2}(g_2(C_1,B_1) + \frac{1}{2}g_0(C_1,B_1)) + \frac{\gamma}{\gamma - 1}(V_x^2 + V_y^2)\left(\frac{\gamma}{\gamma - 1}\frac{1}{\bar{T}}\right)^{1/2}g_0(C_1,B_1) - \frac{2\gamma}{\gamma - 1}(V_x\cos\alpha + V_y\sin\alpha)\,g_1(C_1,B_1)\right\}\right]d\eta d\alpha \tag{29}$$

Note that $C_{\Gamma 1} = C_{\Gamma 1}(\alpha)$, $B_{\Gamma 1} = B_{\Gamma 1}(\alpha)$, and $C_1 = C_1(\alpha,\eta)$, $B_1 = B_1(\alpha,\eta)$ and $\eta_0 = \eta_0(\alpha)$. These equations are written

in terms of the following tabulated functions.[10,11]

$$g_n(C,B) = \int_0^\infty Z^n \exp\left\{-(B - Z)^2 - \frac{C}{Z}\right\} dZ$$

To simplify further discussion, Eq. (26–29) will be written in the following shorthand notation.

$$\pi\bar{\rho} = I_\rho(\bar{\rho},\bar{T},V_xV_y) \tag{26a}$$

$$\pi\bar{\rho}\begin{Bmatrix}V_x\\V_y\end{Bmatrix} = \begin{Bmatrix}I_{vx}\\I_{vy}\end{Bmatrix}(\bar{\rho},\bar{T},V_x,V_y) \tag{27a, 28a}$$

$$\tfrac{3}{2}\pi\bar{\rho}\bar{T} = I_T(\bar{\rho},\bar{T},V_x,V_y) \tag{29a}$$

where the I_ρ, I_{vx}, etc. represent integral operations involving the spatial variations of $\bar{\rho}$, $\bar{T}$, V_x, and V_y.

Equations (26–29) represent four equations in the four unknowns $\bar{\rho}$, $\bar{T}$, V_x, V_y. The distribution function has been eliminated and explicit integration over one of the variables of velocity space (i.e., V) has been accomplished. The problem now reduces to solving these four equations simultaneously. Application of an iterative method of solution is indicated by the complex form of the equations and is discussed in the following section.

Iterative Solution of Four Integral Equations

An initial estimate on the values of $\bar{\rho}$, $\bar{T}$, V_x, V_y is made at every field point. Then a particular point (x,y) is chosen. Through this point, a characteristic of direction α is drawn, and its intersection with the boundary curves noted. From the initial estimate of the flow field, the values of $\bar{\rho}$, $\bar{T}$, etc. are known at every point on the characteristic. This, in turn, permits the integration along that characteristic to be performed. Repeating this process for a range of α's between 0 and 2π, the integrands for the alpha integration are generated. The values of $\bar{\rho}$, $\bar{T}$, V_x and V_y are then obtained by ingration over α. Agreement of the computed and estimated values to within a desired tolerance constitutes convergence. If convergence is not obtained, an improved estimate is made based on the results of the previous iteration and the process repeated until convergence results. A detailed description of the iteration procedure, convergence criteria and method for choosing the initial flowfield distribution is given in Peracchio[7] along with a complete description of the computer program. The flow chart on which the computer program is based is shown in Fig. 2.

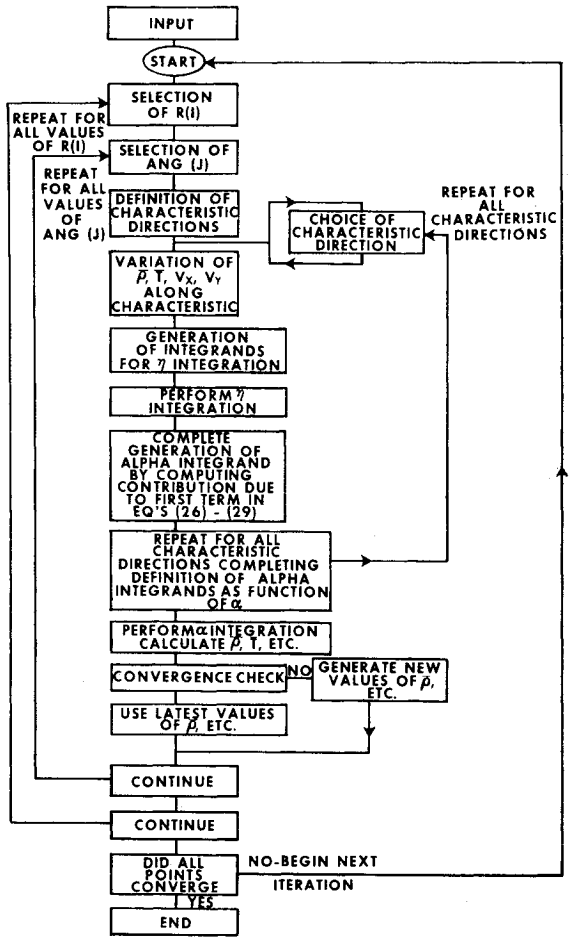

Fig. 2 Major components of program.

Discussion of Results

Preliminary Considerations

The chamber conditions and nozzle exit width, i.e., the nozzle Reynolds number, have been chosen to correspond to a small nozzle whose thrust is in the 1–3 lb range, whose exit Mach number is six and whose chamber temperature is 2000° R. Such a nozzle is typical of the attitude control nozzles required for the stabilization of personalized propulsion units. Since this study is restricted to monatomic gases, a value of $\gamma = 1.667$ was used, and the value of ω for argon in the temperature-viscosity relationship was chosen.[12] Application of the results to other monatomic gases with the same value of ω is possible if the nozzle Reynolds numbers are the same.

The program was run for two thrust levels, or Reynolds numbers. The thrust levels, assuming a square nozzle exit shape whose width is $2L$, are 2 and 1 pound. The corresponding values of Re_0 are 0.436×10^4 and 0.218×10^4. A summary of the nozzle chamber and exit conditions is shown in Table 1.

The initial estimate for the flowfield was based on the isentropic flow solution and the results of some preliminary

Table 1 Nozzle chamber and exit conditions

$\gamma = 1.667$
Exit Mach number $= 6.0$
$\bar{T}_\Gamma = 0.0769$
$\bar{\rho}_\Gamma = 0.02134$
$\bar{V}_{y\Gamma} = 0.961$

Case	Thrust (lb)	Re_0	P_0 (psia)
1	2	0.436×10^4	1.2
2	1	0.218×10^4	0.6

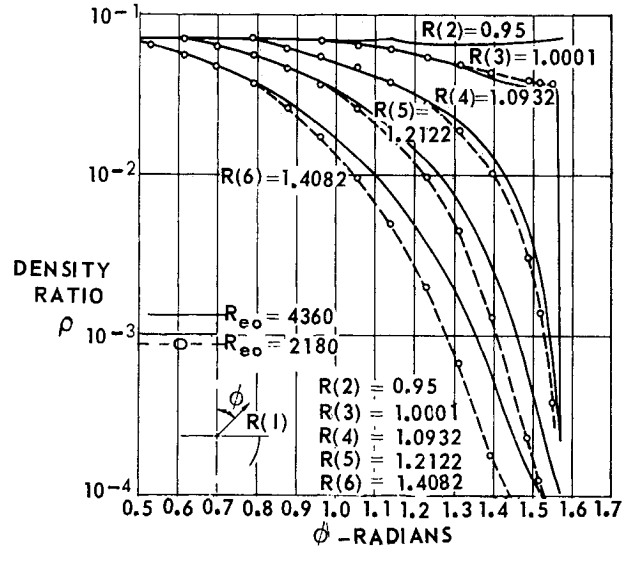

Fig. 3 Density ratio vs angle ϕ for constant values of radius.

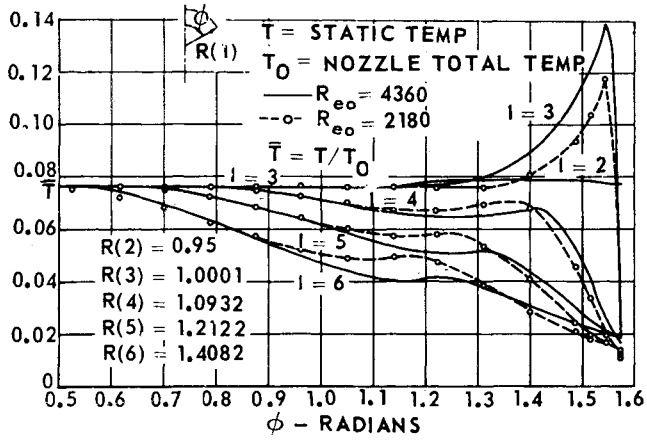

Fig. 4 Temp ratio vs angle ϕ.

runs. The solution was obtained for the upper half plane, since this is the region of primary interest.

Results

Convergence to within 0.5% for $\bar{\rho}$, $\bar{T}$, V_x, and V_y at all points of the flowfield required 10 iterations for the case in which $Re_0 = 4360$ and 9 for $Re_0 = 2180$. Running time on the UNIVAC 1108 for the 10 iterations was on the order of one hour. The resulting values of $\bar{\rho}$ and $\bar{T}$ for both cases are plotted in Figs. 3 and 4 as a function of the angle ϕ [or $ANG(J)$] for the 5 following values of radius, i.e., $R(2) = 0.95$, $R(3) = 1.0001$, $R(4) = 1.093$, $R(5) = 1.2122$, $R(6) = 1.4082$.

The magnitude of the macroscopic velocity vector divided by V_0 is plotted in Fig. 5, and the angle, μ, between the velocity vector and the axis in Fig. 6. Contour plots of $\bar{\rho}$, $\bar{T}$, $|\mathbf{V}_0|/V_0$ and μ are also shown for the case with $Re_0 = 4360$ in Fig. 7 through Fig. 10. Superimposed on these contour plots is the isentropic solution for an exit Mach number of 6. Since the isentropic solution is defined by the flow properties of a Prandtl-Meyer turn, $\bar{\rho}$, $\bar{T}$, etc. are constant along rays emanating from the nozzle corner. The rays corresponding to the first Mach wave and the zero pressure stream surface are shown fully drawn. Property values for intermediate rays are obtained by aligning the appropriate ray segment with the corner of the nozzle. For example, in Fig. 7, the ray along which $\bar{\rho} = 0.00497$ is obtained by extension of the 0.00497 ray segment to the nozzle corner.

Discussion

Considering first Fig. 3, the qualitative behavior of the density is as expected. For a given radius, the density falls off as the azimuthal angle ϕ sweeps from the nozzle centerline toward the horizontal axis. In addition, for a given value of ϕ, the density is seen to drop as the radius increases. The isentropic solution is indicated in the contour plot of Fig. 7. The deviations from the isentropic are two-fold in nature. First, in the area between the first Mach wave and the nozzle centerline, but in the vicinity of the Mach wave, the isentropic solution predicts a constant density. The kinetic theory solution, however, is seen to result in slightly lower values of density, which propagate into the constant density region. This is best explained by considering the contribution to a typical point of a right running characteristic which passes out into the low density regions of the flowfield, as shown in Fig. 11. If $\bar{A}$ were extremely large, the density would depend only on the property values in the immediate vicinity of the point, as shown by the smaller circle a. As $\bar{A}$ decreases, the circle increases in size until at some radius, indicated by circle b, the contribution to $\bar{\rho}$ due to the indicated characteristic is decreased due to its passage through a lower density region. The mirror image of the indicated characteristic remains in the constant density region, hence its contribution is not decreased. This "relief" mechanism is responsible for the indicated deviation from the isentropic solution in the vicinity of the first Mach wave and applies to the deviations in temperature and velocity as well.

The second deviation occurs in the lower density regions of the plume, where the kinetic theory solution predicts larger values than the isentropic. This behavior is expected, since the isentropic solution predicts zero property values outside the free streamline whereas, in reality, molecules are scattered into this region through collisions from the higher density regions of the flowfield. This scattering mechanism is present in the BGK equation, as indicated by the existence of a solution beyond the zero-pressure streamline, and is responsible for the higher values of density.

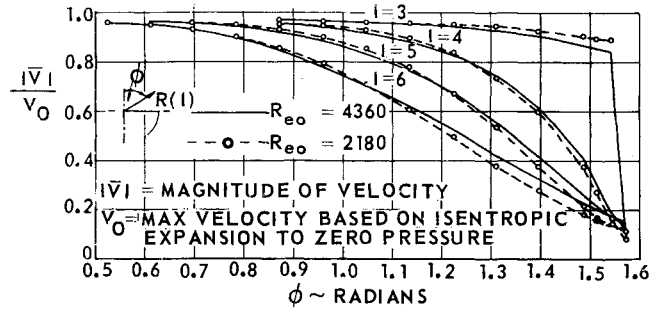

Fig. 5 Velocity magnitude vs angle ϕ.

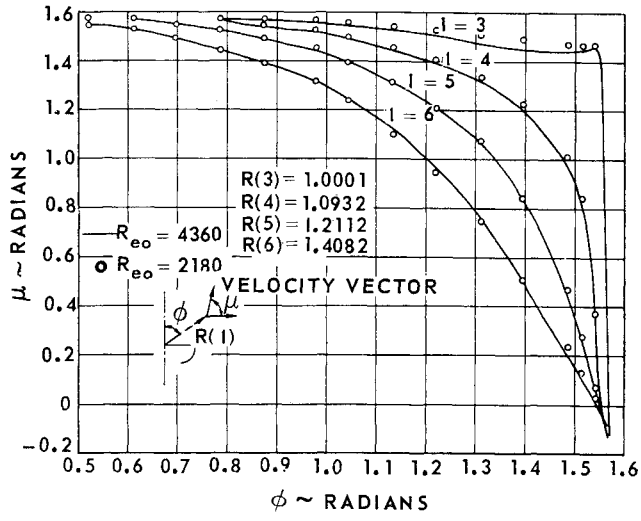

Fig. 6 Angle μ between velocity vector and x axis vs ϕ.

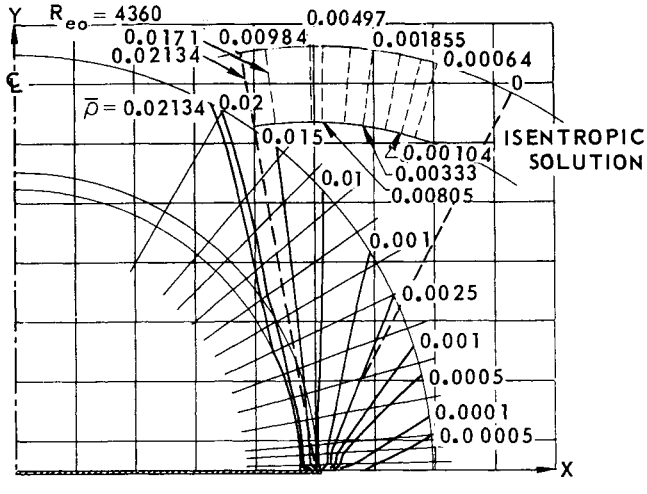

Fig. 7 Contour plot—density, $\bar{\rho}$.

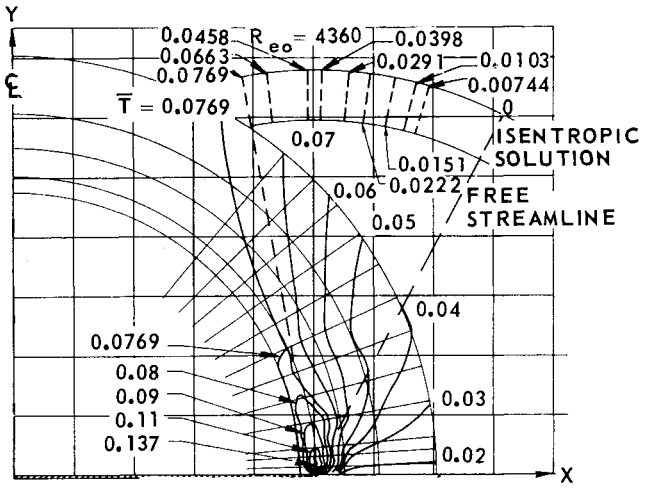

Fig. 8 Contour plot—temperature — $\bar{T}$.

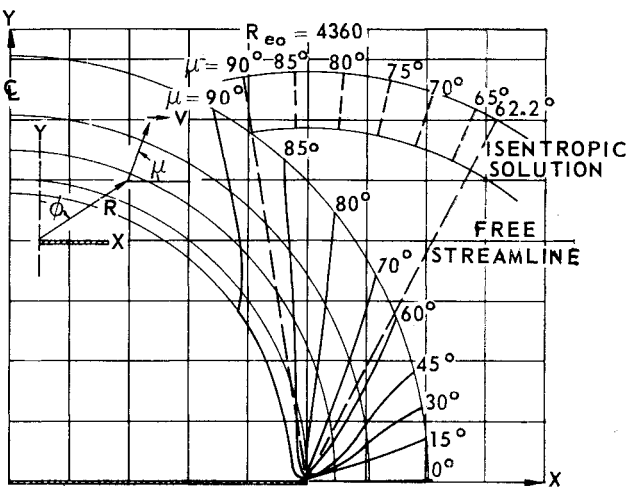

Fig. 10 Contour plot—angle μ between velocity vector and axis.

The behavior of the static temperature is somewhat unexpected in that a rise occurs near the corner of the nozzle, as shown in Fig. 8. It is interesting to note that this rise occurs in the region of the flowfield that exhibits the largest property gradients. It is shown by Peracchio[7] that significant deviations from continuum prediction result when property gradients are high, even if $\bar{A}$ is large.

It must therefore be concluded that the exhibited temperature rise occurs in an area that deviates significantly from the continuum and is caused by the effects of heat transfer and viscosity. Qualitatively, a similar behavior is observed in a boundary layer adjacent to an adiabatic wall, where, due to viscous shear and heat transfer, the magnitude of velocity decays rapidly to zero while the static temperature increases. The flow near the corner of the nozzle is seen to exhibit this behavior also, as shown in Figs. 8 and 9. The velocity magnitude decays rapidly near the nozzle corner while, concurrently, the temperature exhibits a rapid rise.

Further evidence that the flow is in the noncontinuum regime near the corner of the nozzle is afforded by the distribution function. For a Maxwellian distribution function, or one close to it, the Euler or Navier-Stokes equations would be valid, and the flow would be in the continuum regime. Significant deviations, on the other hand, indicate large departures from the continuum regime and therefore large viscous and heat-transfer effects. Since the result of the integration along a characteristic is available as a function of α from the program, a comparison of the actual and Maxwellian distribution functions is possible. The local Maxwellian is written in terms of (V,α), and then integrated over V for comparison with the actual distribution function. Defining this integral to be $\mathfrak{F}$, the partial distribution function, there results for the Maxwellian,

$$\mathfrak{F}_m(\alpha) = \bar{\rho} g_1 \left[0, \left(\frac{\gamma}{\gamma-1}\frac{1}{\bar{T}}\right)^{1/2}\left\{V_x \cos\alpha + V_y \sin\alpha\right\}\right] \times \exp\left\{-\frac{\gamma}{\gamma-1}\frac{1}{\bar{T}}(V_x \sin\alpha - V_y \cos\alpha)^2\right\}$$

where $\bar{\rho}$, $\bar{T}$, V_x and V_y are the local values at the point in question.

The actual and Maxwellian partial distribution functions are compared in Fig. 12 for the point $R(I)$ = 1.0001 and $ANG(J)$ = 1.5417 radians, which exhibited the largest value of $\bar{T}$. As is clearly shown, the actual distribution function deviates significantly from the Maxwellian, indicating large departure from the continuum, and therefore significant effects due to shear stress and heat transfer.

The direction of the macroscopic velocity vector, as shown in Fig. 10, tends to follow the isentropic solution except in the vicinity of the nozzle corner where deviations occur because of the large gradients, and in the vicinity of the free streamline and beyond, where the isentropic flowfield is nonexistent. The qualitative behavior beyond the free streamline is as expected, in that the angle between the velocity vector and the x

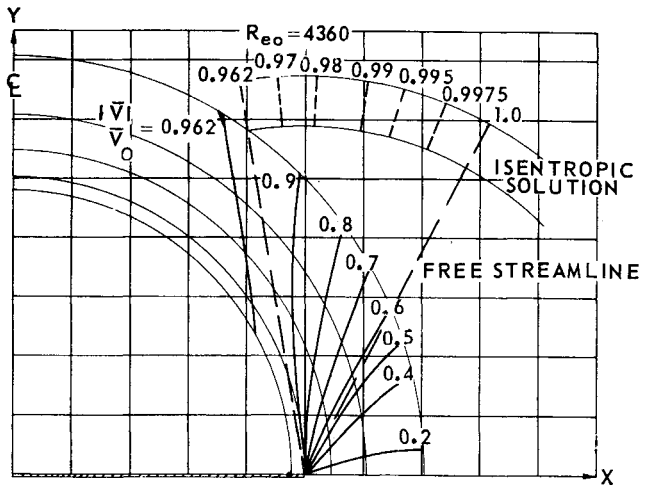

Fig. 9 Contour plot—velocity magnitude — $|\bar{V}_0|/V_0$.

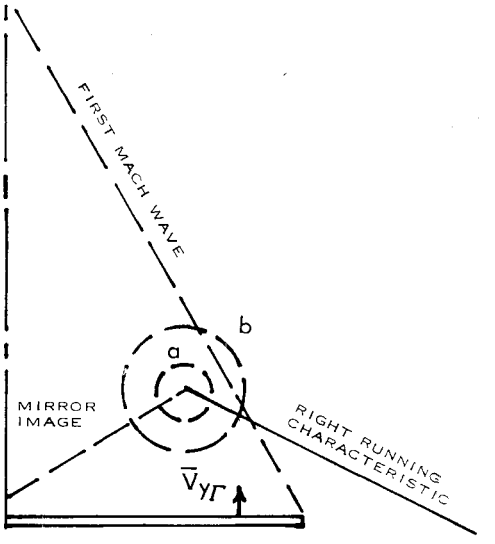

Fig. 11 Right running characteristic.

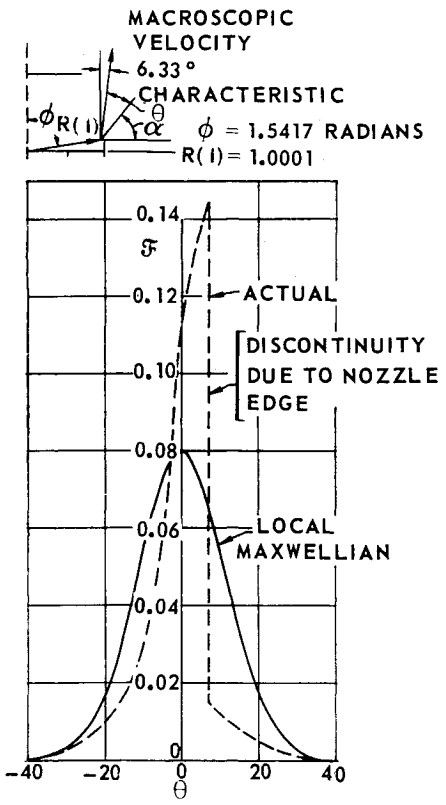

Fig. 12 Comparison of partial distribution functions.

axis decays monotonically with ϕ for any radius and with radius, for any ϕ (see also Fig. 6).

The magnitude of the velocity vector is shown in the contour plot of Fig. 9. Its behavior is opposite to the isentropic solution in that its magnitude decreases while the velocity magnitude predicted by the isentropic solution increases slightly from 0.962 to the theoretical maximum of 1 at the free streamline. The actual solution for $|\mathbf{V}_0|/V_0$ in the vicinity of the free streamline is on the order of 0.6, and represents a 40% reduction from the isentropic value. This deviation is less pronounced in the higher density regions of the flowfield.

Thus the solution based on the BGK equation deviates from the isentropic, predicts property values beyond the zero pressure streamline and a "relief" effect which results in small deviations from the isentropic even in the vicinity of the first Mach wave, in the area between the Mach wave and the nozzle centerline. In the low density or low collision frequency regions, the deviations increase, with decreasing density, and in addition, significant deviations, especially in temperature, occur near the corner of the nozzle where large property gradients exist.

Comparison of the results for the two nozzle Reynolds numbers, as shown in Fig. 3 through Fig. 6, indicates that the two solutions have the same qualitative behavior. The density comparisons (Fig. 3) show that for a given radius, the density plots follow each other until a value of $\bar{\rho}$ on the order of 0.01 is reached, at which point the density for the lower Reynolds number case decays more rapidly as ϕ increases. This behavior is due to the lower collision frequency which results from the lower value of Re_0. Since the collision frequency is lower in the high density regions of the flow for the $Re_0 = 2180$ case, fewer molecules can be scattered into the outer regions of the flowfield, the result being a lower density. The temperature comparison of Fig. 4 indicates the same qualitative behavior for the two cases, although for $Re_0 = 2180$, the peak temperature in the corner of the nozzle is less.

Partial verification of the numerical efficacy of the program was obtained by a continuity check. The mass flow passing each of the radii $R(I)$ was computed for both solutions and compared to the mass flow leaving the nozzle exit. Agreement to within 1.4% resulted.

Conclusions

The application of the BGK equation to the solution for the flowfield of a two-dimensional nozzle exhausting into a vacuum has been accomplished, and it indicates that:

1) The flowfield exists beyond the free streamline predicted by the isentropic solution, as anticipated.

2) Deviations from the isentropic solution occur due to the presence of both low collision frequencies and large property gradients.

3) An unexpected rise in static temperature occurs in the vicinity of the nozzle edge due to the large property gradients and deviations from the continuum.

References

[1] Edwards, R. H. and Rogers, A. W., "Steady Non-Isentropic Jet Expansion into a Vacuum," AIAA Paper 66-490, Los Angeles, Calif., June 1966.

[2] Edwards, R. H. and Cheng, H. K., "Steady Expansion of a Gas into a Vacuum," *AIAA Journal*, Vol. 4, No. 3, March 1966, pp. 558–561.

[3] Hamel, B. B. and Willis, D. R., "Kinetic Theory of Source Flow Expansion with Application to the Free Jet," *The Physics of Fluids*, Vol. 9, No. 5, May 1966, pp. 829–841.

[4] Brook, J. W. and Oman, R. A., "Steady Expansions at High-Speed Ratio Using the BGK Kinetic Model," *Rarefied Gas Dynamics, Proceedings of the 4th Symposium*, Vol. I, Academic Press, 1965, pp. 125–139.

[5] Bhatnagar, P. L., Gross, E. P., and Krook, M., "A Model for Collision Processes in Gases. Part I. Small Amplitude Processes in Charged and Neutral One-Component Systems," *Physical Review*, Vol. 94, No. 3, May 1954, pp. 511–525.

[6] Vincente, W. G. and Kruger, C. H., *Introduction to Physical Gas Dynamics*, Wiley, New York, 1965.

[7] Peracchio, A. A., "Kinetic Theory Analysis of the Flow Field of a Two-Dimensional Nozzle Exhausting to Vacuum," Ph.D thesis, Rensselaer Polytechnic Institute, Troy, N. Y., May 1968.

[8] Chu, C. K., "Kinetic Theoretic Description of the Formation of a Shock Wave," *The Physics of Fluids*, Vol. 8, No. 1, Jan. 1965, pp. 12–22.

[9] Anderson, D. G., "On the Steady Krook Equation: Part 1" *Journal of Fluid Mechanics*, Vol. 26, Part 1, Sept. 1966, pp. 17–35.

[10] Anderson, D. G., and Macomber, H. K., "Evaluation of $\frac{1}{(2\pi)^{1/2}} \int_0^\infty du u^{n-2} \exp\left\{-\frac{1}{2}(u-p)^2 - q/u\right\}$" *Journal of Mathematics and Physics*, Vol. 55, No. 1, March 1966, pp. 109–120.

[11] Chahine, M. T. and Narasimha, R., "Evaluation of the Integral $\int_0^\infty V^n \exp[-(V-u)^2 - x/v]dV$" TR 32-459, Aug. 1963, Jet Propulsion Lab., Pasadena, Calif.

[12] Hanley, H. J. M., "The Viscosity and Thermal Conductivity Coefficients of Dilute Argon Between 100 and 2000° K," TN 333, 1966, National Bureau of Standards.